



In-situ analysis of nucleation reactions during TiCl₄/H₂O Atomic Layer Deposition on SiO₂ and H-terminated Si surfaces treated with a silane small molecule inhibitor

Jan-Willem J. Clerix^{a,b,c,+,#}, Golnaz Dianat^{a,#}, Annelies Delabie^{b,c}, Gregory N. Parsons^{a,*}

^a Department of Chemical and Biomolecular Engineering, 911 Partners Way, Raleigh, NC 27606, USA

^b Department of Chemistry, KU Leuven, Celestijnenlaan 200F, 3001 Heverlee, Belgium

^c imec, Kapeldreef 75, 3001 Heverlee, Belgium

[#] JJC and GD are joined first authors of this manuscript

^{*} Corresponding autho: gnp@ncsu.edu

⁺ Current address: BASF, Scheldelaan 600, 2000 Antwerpen, Belgium

ABSTRACT

Small molecule inhibitors (SMIs) have recently been introduced for passivation during area-selective deposition (ASD). Small silanes like (N,N-dimethylamino)trimethylsilane (DMATMS) selectively react with OH sites on SiO₂ to form a less reactive -OSi(CH₃)₃ terminated surface. The -OSi(CH₃)₃ surface termination can inhibit many atomic layer deposition (ALD) processes, including TiCl₄/H₂O ALD. However, the mechanisms by which ALD is inhibited, and by which selectivity is eventually lost are not well understood. This study uses in-situ Fourier-transform infrared spectroscopy (FTIR) to probe the adsorption of DMATMS on SiO₂, and the subsequent reactions when the passivated surface is exposed to TiCl₄/H₂O ALD. The chemisorption of DMATMS on isolated -OH groups on SiO₂ is shown to inhibit reaction with TiCl₄. Further, we find that starting with an inherently-inhibiting H-terminated Si surface, DMATMS can also react with residual -OH groups and reduce the extent of nucleation. Finally, using Rutherford backscattering spectrometry (RBS), the effectiveness of DMATMS passivation on SiO₂ and H-terminated Si is quantified during extended ALD cycle numbers. The insight into the mechanisms of passivation by DMATMS and passivation loss can enable the rational design of highly selective ASD processes by carefully matching compatible surfaces, passivating agents and ALD precursors.

I. INTRODUCTION

Area-selective deposition (ASD) is a recent approach to simplify future semiconductor device manufacturing. ASD is typically performed on prepatterned substrates by selectively depositing a material on a growth area while avoiding growth on an adjacent non-growth area. Through this approach, patterns can be replicated with high accuracy.¹ A sequence of passivation, deposition and etch, possibly in supercycles, has become a preferred approach in highly selective ASD process development.² Passivation is typically achieved by self-assembled monolayers (SAMs), or small-molecule inhibitors (SMIs).¹ Though the introduction of SMIs is recent, they have come to be seen as a promising candidate for passivation in ASD of complex 3D structures.³ SAMs are typically inert and are able to form physical barriers against precursor diffusion. Though SAMs have been used to enable ASD for the fully-self aligned via, they are restricted by a number of compatibility issues.⁴⁻⁸ First, they are often deposited from solution, or through slow vapor phase deposition. Second, most SAMs are only stable at low temperatures, which restricts use to ASD of metal oxides, as metals are often deposited at

too high temperatures. Thirdly, the undesired and often uncontrolled deposition of multilayers complicates usage in nanopatterns. A final issue is shadowing of the growth area by lying-down SAM molecules that extend laterally at the junction between growth and non-growth regions, or due to the relatively large size (1.5-2 nm) of SAM molecules compared to semiconductor feature dimensions (~10 nm). In contrast to SAMs, SMIs are typically deposited quickly from the vapor phase, and can often be deposited in atomic layer deposition (ALD) and chemical vapor deposition (CVD) tools. Such rapid deposition makes them ideally suited for application in supercycles to increase ASD film thicknesses.^{9, 10} SMIs of the small silanes family, as studied here, bind strongly to -OH sites on SiO₂ surfaces and are stable to temperatures well above most ALD temperature windows.¹¹ As such, small silanes are analogous to ALD precursors in that they react via a self-limiting reaction with available -OH groups on SiO₂, thereby preventing the shadowing of the growth area on the patterned substrate.^{10, 12}

(N,N-dimethylamino)trimethylsilane (DMATMS) is an SMI from the family of small silanes. DMATMS reacts with surface -OH groups on SiO₂ to form a -OSi(CH₃)₃ surface termination and volatile HN(CH₃)₂. The -OSi(CH₃)₃ termination is stable to over 600 °C.¹¹ By eliminating or shielding -OH groups, which are typical reactive sites during many ALD processes, it renders the surface hydrophobic and less reactive during ALD. The -OSi(CH₃)₃ termination has been shown to be a good inhibitor in noble metal ALD of Ru and Pt from metalorganic precursors on SiO₂.^{10, 12-14} Metal oxide ALD of TiO₂, TiN and Al₂O₃ is also inhibited on DMATMS-treated SiO₂.¹⁵ In addition, DMATMS has been used to increase selectivity in the selective CVD of Mn and Ru.^{16, 17} Xu et al. recently studied DMATMS as a secondary passivation agent, in combination with bis(dimethylamino)dimethylsilane (BDMADMS).^{18, 19} They showed that during (dimethyl)aluminum(isopropoxide)/H₂O ALD, growth on the doubly-passivated SiO₂ is inhibited by competition for surface -OH groups. However, the reactivity of different types of -OH groups to DMATMS deposited from the vapor phase could not be elucidated. Inhibition loss during ALD could be explained by physisorption of the Al-precursor on siloxane bridges. Interestingly, DMATMS has been shown to be well-suited for the passivation of polymers with isolated -OH groups during TiO₂ ASD.²⁰ DMATMS adsorption can also improve selectivity by mechanisms other than reaction passivation. Grillo et al. showed that in the case of Ru CVD, DMATMS adsorption on nanopatterned surfaces enhances surface diffusion of physisorbed precursors from the non-growth area to the growth area, thereby enhancing selectivity.¹⁷

The mechanisms by which SMIs, such as DMATMS, inhibit ALD growth on specific surfaces are poorly understood.³ Inhibition has been demonstrated to be due to adsorption on and consumption of reactive sites, and/or through diffusion of adspecies.^{3, 17} Inhibition loss has been attributed to SMI configuration on the surface, limited surface coverage and reactions between the SMI and ALD precursors.^{9, 21-24} To improve our understanding of inhibition and inhibition loss mechanisms, and with the end goal of improving selectivity of metal oxide ASD, we investigate the interactions of DMATMS with SiO₂, and with TiCl₄ and H₂O as ALD precursors. These mechanisms are compared to the mechanisms of TiCl₄/H₂O ALD on the inherently inhibiting H-terminated Si. The potential for inhibition enhancement by addition of DMATMS to H-terminated Si is explored. We used in-situ Fourier-transform infrared spectroscopy (FTIR) to characterize changes in surface chemistry, while Rutherford backscattering spectrometry (RBS) was used to determine growth rates. The obtained insights are used to discuss selectivity improvements for metal oxide ASD process design.



II. METHODS

(N,N-dimethylamino)trimethylsilane (DMATMS) (Fisher Scientific, 97%) was used as the inhibitor, Titanium tetrachloride (TiCl_4) (Gelest, 99%) was used as Ti-precursor, and deionized water was used as the oxygen source.

For RBS studies, planar double-side-polished p-type (100) wafers with resistivity of 30-60 Ω cm were cut in small 1x3 cm^2 pieces and piranha (1:1 H_2SO_4 : H_2O_2) cleaned to remove the organic contamination and form a hydrophilic hydroxyl-terminated (SiO_2) surface. To obtain a hydrophobic hydrogen-terminated (H-terminated Si) surface, the substrates were dipped into 5% HF solution for 30 seconds. For in-situ FTIR measurements porous silicon substrates were used to enhance absorbance intensity. To prepare porous hydrogen-terminated silicon substrates, double-side-polished p-type (100) wafers with resistivity of 30-60 Ω cm were electrochemically etched in 50% aqueous HF and 99.8% ethanol 1:1 solution for 20 minutes at a current density of 14 mA/cm^2 .²⁵ To obtain hydroxyl-terminated porous silicon substrates, the resulting Si-H porous wafers were held in hydrogen peroxide (H_2O_2 , 30% in water) at room temperature for 60 minutes and then stored in water. The resulting high-surface area silicon substrates are referred to as “porous H-terminated Si” and “porous SiO_2 ”.

ALD deposition studies were carried out in a lab-built ALD system, described previously, equipped with in-situ Fourier transform infrared spectroscopy (FTIR) in transmission configuration.^{26, 27} For FTIR studies, porous silicon substrates were mounted on a sample holder with mounted cartridge heaters to heat the samples to 250 $^\circ\text{C}$. Both the DMATMS deposition and the $\text{TiCl}_4/\text{H}_2\text{O}$ ALD process occur readily at 250 $^\circ\text{C}$. Nitrogen was used as a carrier and purging gas, resulting in an operating pressure of 500 mTorr N_2 during both purging and precursor exposure. During the deposition and the measurement, reactor walls and delivery lines were held at 100 $^\circ\text{C}$ and 60 $^\circ\text{C}$, respectively. TiO_2 was deposited onto hydroxylated SiO_2 and H-terminated Si, and hydroxylated SiO_2 and H-terminated Si surfaces that were exposed to 60 cycles of DMATMS. A cycle of DMATMS consisted of a single 1s dose of DMATMS, with a 35s N_2 purge. A cycle of TiO_2 ALD consisted of a 1s dose of TiCl_4 , a 60s N_2 purge, a 1s dose of H_2O , and a final 60s N_2 purge. Each FTIR spectrum was collected after five 1s subdoses of a reactant, separated by 60 s of N_2 purge, using a Thermo Fisher Nicolet 6700 spectrometer and an MCT-A external detector. The measurements were acquired with a resolution of 6 cm^{-1} in a range of 650-4000 cm^{-1} and averaged over 512 scans. The integrated area values under -OH peaks of the FTIR absorbance spectrum of the growing TiO_2 films are calculated using integration with baseline function in SpectraGryph 1.2 software. TiO_2 deposition on planar substrates was quantified by RBS, using a 1.523 MeV He^+ ion beam. The TiO_2 thickness was calculated from the RBS data by assuming the TiO_2 bulk density of 4.238 g cm^{-3} , which translates to a $3.19 \cdot 10^{22}$ Ti atoms cm^{-2} . The RBS-derived thickness was verified by spectroscopic ellipsometry for SiO_2 and H-terminated Si samples after 60 cycles DMATMS and 100 cycles TiO_2 ALD. For SiO_2 this resulted in a TiO_2 thickness of 0.8 nm for RBS, and 0.9 nm for ellipsometry. For H-terminated Si this resulted in 0.5 nm for RBS, and 0.4 nm for ellipsometry. These results support the validity of the RBS-derived thicknesses.

III. RESULTS AND DISCUSSION

A. DMATMS Reactions on Hydroxylated SiO_2

To understand the interaction of DMATMS molecules with the SiO_2 surface, we performed in-situ FTIR analysis and monitored vibrational modes of the chemical species at the surface of the porous SiO_2 substrate at 250 $^\circ\text{C}$ for different numbers of DMATMS cycles. The identification of all FTIR peaks is mentioned in Table I. The FTIR spectrum of the hydroxylated porous SiO_2 surface before DMATMS exposure is shown in Figure 1a. After 5 cycles of

DMATMS exposure, the differential infrared spectrum shows a sharp negative peak at 3735 cm^{-1} indicating that DMATMS reacts with isolated surface hydroxyl groups (Figure 1b). The broad negative-going shoulder of this peak between ~ 3700 and 3400 cm^{-1} indicates reaction with H-bonded -OH groups. The differential FTIR spectrum also shows the formation of Si-O-Si bonds (1088 cm^{-1}), as well as the appearance of C-H stretching (2961 cm^{-1}), and Si-CH₃ stretch and rocking vibrations (759 cm^{-1} , 848 cm^{-1} and 1258 cm^{-1}). These increases in vibration indicate that the surface becomes -OSi(CH₃)₃ terminated by the reaction of DMATMS with mainly isolated and some H-bonded surface -OH groups.

To examine the extent of saturation, the porous SiO₂ was exposed to 55 additional cycles of DMATMS, for a total of 60 cycles. This experiment shows that the reaction of DMATMS with the SiO₂ surface is fast, as indicated by the extent of the reaction after 5 cycles (Figure 1c). However, the -CH₃ stretch continues to increase and saturation is achieved after ~ 25 cycles, as can be seen in Figure 1 d. After a total of 60 cycles, the integral of the Si-CH₃ peak increases by only 30% compared to after 5 cycles. To quantify the fraction of surface -OH groups that react with DMATMS, the integrated area under the broad peak associated with all surface -OH groups (O-H stretch at $3760\text{-}3400 \text{ cm}^{-1}$) was calculated before and after reaction with DMATMS. This analysis shows that the first 5 cycles remove only 16% of the total amount of -OH groups, and after 60 cycles, a total of 29% is removed. However, the sharp peak associated with isolated -OH groups (O-H stretch at $3760\text{-}3698 \text{ cm}^{-1}$) disappears after 60 cycles, indicating that most of these groups react with DMATMS. It should also be noted that the -OH peak might contain a number of -OH groups which are not accessible to DMATMS due to the tightness of the pore size and therefore cannot be passivated. To ensure that all surface sites that react with DMATMS have been passivated, DMATMS was dosed for 60 cycles in all subsequent experiments.

As discussed, a significant portion of the H-bonded -OH groups do not react with DMATMS. This means that unwanted ALD may be able to proceed if the ALD precursors can react with the residual -OH groups that are not sterically shielded by the -OSi(CH₃)₃ termination.

Table 1 Relevant FTIR peaks with identification.

Wavenumber (cm^{-1})	Identification	Reference
665	Si-H	28
760	Ti-O-Ti	29
810	Si-O	
850	Si-O-Si	30
914	Si-O in SiO ₂ -TiCl ₂	29, 31
916	Si-H ₂	28
1014	Si-O in SiO-TiCl ₃	32
1088	Si-O-Si	31, 33
1258	Si-CH ₃	31
2100	Si-H _x	31, 34
2961	C-H	27, 34, 35
3550	Strong H-bonded O-H	36
3650	Weak H-bonded O-H	36
3735	Isolated O-H	29, 36, 37

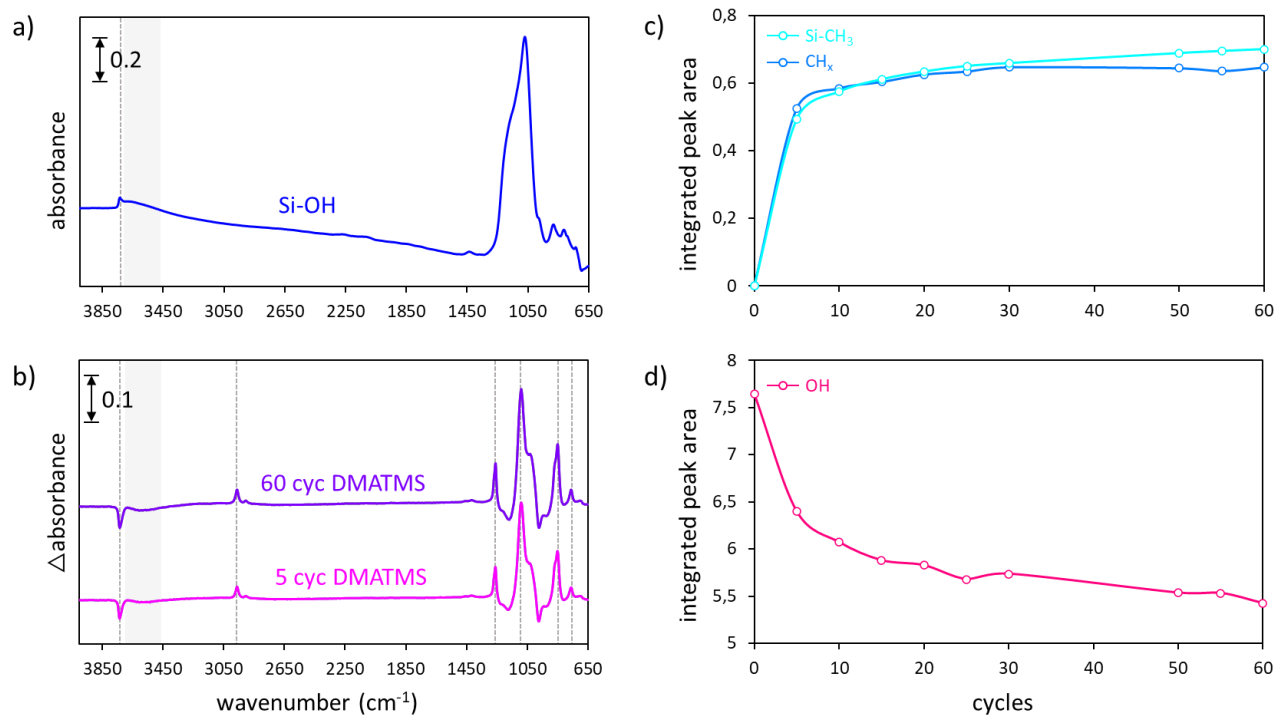


Figure 1. a) FTIR spectrum of starting SiO₂ surface, b) Differential FTIR spectra of the SiO₂ surface after 5 or 60 cycles DMATMS, integrated area under c) Integrated area of the SiCH₃ peak between 1282-1248 cm⁻¹ and CH_x peak between 2930-2996 cm⁻¹ as function of DMATMS cycles and, (d) Integrated area of the -OH peak between 3400-3760 cm⁻¹ as function of DMATMS cycles.

B. Surface reactions during the first TiCl₄/H₂O ALD cycle on SiO₂

To better understand how DMATMS treatment inhibits TiO₂ ALD on hydroxylated SiO₂, we first study the reactions of TiCl₄ and H₂O with the as-formed non-passivated SiO₂ substrate (Figure 2b). FTIR spectra are collected after each half reaction. The initial reaction of TiCl₄ is marked by the nearly complete disappearance of the broad peak associated with -OH groups on the surface (3760-3400 cm⁻¹). 86% of the initial surface -OH groups are consumed by reaction with TiCl₄, as indicated by the integrated areas under this peak (Figure 2b). This includes isolated as well as H-bonded -OH groups. The remaining 14% of the -OH groups are not available for reaction, either due to steric hindrance by the Cl-ligands or they are unavailable due to the pore size and therefore not accessible to the ALD precursors. The reaction between -OH and TiCl₄ creates surface Ti-species that are singly (914 cm⁻¹) or doubly (1014 cm⁻¹) bound to the SiO₂ surface. Exposure to H₂O in the second half-cycle creates new Ti-OH groups, but the reaction is limited in extent and after the first H₂O half-cycle the amount of -OH groups is equal to only 29% of the initial amount on the starting surface. The reduced number of -OH sites after the first ALD cycle leads to lower growth rates in the subsequent cycles. This decrease in growth rate after the first cycle has previously been described for TiCl₄/H₂O ALD.^{25, 36}

The enhanced TiCl₄ adsorption in the first cycle implies a significant fraction of the TiO₂ islands that will finally form the TiO₂ film nucleate in the first ALD cycle. It is therefore most important to curb TiCl₄ adsorption during the first ALD cycle and doing so effectively should reduce the number of undesired islands on the non-growth area.

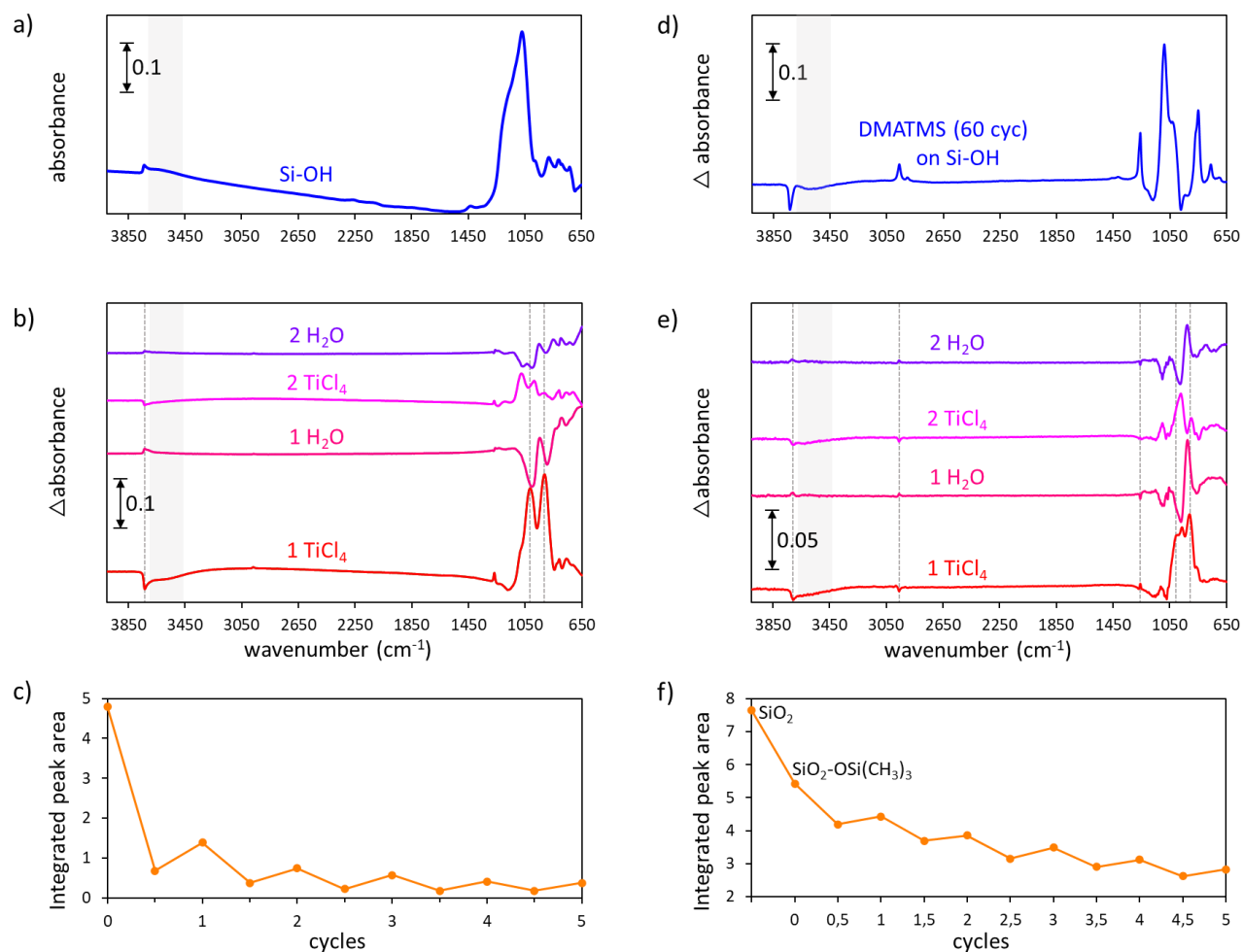


Figure 2. a) FTIR spectrum of starting SiO₂ surface, b) differential FTIR spectra of the SiO₂ surface after TiCl₄ and H₂O half-cycles during the first 2 TiO₂ ALD cycles, c) integrated area under OH peak between 3400-3760 cm⁻¹ of growing TiO₂ on the SiO₂ surface as function of TiCl₄/H₂O ALD cycles. d) FTIR spectrum after 60 cycles of DMATMS on the SiO₂. e) differential spectra after TiCl₄ and H₂O half-cycles during the first 2 TiO₂ ALD cycles on SiO₂-Si(CH₃)₃ f) integrated area under OH peak between 3400-3760 cm⁻¹ of growing TiO₂ on the SiO₂-Si(CH₃)₃ surface as function of TiCl₄/H₂O ALD cycles.

C. Surface reactions during the first TiCl₄/H₂O ALD cycle on passivated SiO₂

To understand the initial growth of TiO₂ on DMATMS-passivated SiO₂, the experiment above was repeated on a hydroxylated SiO₂ surface that was first exposed to 60 cycles of DMATMS. As discussed above, 71% of the initial -OH groups remain on the surface after 60 cycles of DMATMS from the integrated area under the -OH peak, but many of the remaining -OH sites are expected to be adjacent to bound DMATMS where steric hindrance can make them inaccessible for reaction with TiCl₄. After the first TiCl₄ exposure, the differential FTIR spectrum shows a negative peak at 3760-3400 cm⁻¹, which indicates that some of the residual -OH groups are still able to react with TiCl₄, in spite of the passivation (Figure 2e). The first TiCl₄ exposure reacts with ~23% of available surface -OH groups (Figure 2f). The ~77% unreacted -OH groups are either sterically shielded or interstitial. The peaks associated with TiCl₄ absorption (1014 cm⁻¹, 914 cm⁻¹) are much smaller than on the non-passivated SiO₂, which indicates that the TiCl₄ reaction is much less extensive than on the non-passivated surface. Exact quantitative comparison is not possible due to variability between porous substrates. It is also clear that the peak absorbance of the consumed -OH groups is found at a lower wavenumber (3705 cm⁻¹ instead of 3735 cm⁻¹). This indicates that no observable isolated -OH groups (3735 cm⁻¹) are present on the surface for reaction with TiCl₄, after

DMATMS treatment. Instead, the peak absorbance corresponds to weakly H-bonded -OH groups.

TiCl₄ reacts primarily with H-bonded -OH groups, since all isolated -OH groups are effectively passivated by DMATMS. The reaction with H-bonded -OH groups increases the likelihood of a bifunctional reaction, resulting in the preferential formation of SiO₂-TiCl₂ over SiO-TiCl₃. This is indeed supported by the very weak distinct peak at 1014 cm⁻¹, which is associated with SiO-TiCl₃.

The first H₂O exposure creates Ti-OH groups, but again fewer -OH groups are created than were consumed in the first TiCl₄ exposure. The more limited extent of rehydroxylation on the passivated SiO₂ can also be related to the bifunctional reaction of TiCl₄ on the passivated SiO₂ surface. The dominant Ti species on the surface are SiO₂-TiCl₂ on the passivated SiO₂ surface instead of SiO₂-TiCl₂ and SiO-TiCl₃ on the non-passivated SiO₂ surface. Therefore, fewer -Cl groups are available for hydrolysis on the passivated SiO₂ surface.

The reduced TiCl₄ adsorption during the first cycle will result in fewer TiO₂ nuclei on the surface for subsequent (undesired) growth. Since metal oxide nuclei are expected to grow at a constant rate, layer closure of TiO₂ should be significantly delayed.^{38, 39} Interestingly, the limited formation of -OH groups in the first ALD cycle might limit further Ti uptake in the subsequent cycles, which could result in a persisting inhibition during TiO₂ ALD. The latter explains observations by Nye et al., who saw that in spite of enhanced TiCl₄ adsorption on DMATMS-passivated SiO₂ in the first ALD cycle, the formed nuclei grew at a lower GPC value than expected.²⁴

D. Inhibition loss mechanisms on passivated SiO₂

Inhibition of TiO₂ ALD on DMATMS-treated SiO₂ is lost through two mechanisms. In the first mechanism, TiCl₄ reacts with H-bonded -OH, which are poorly passivated by DMATMS. Even though the -OSi(CH₃)₃ surface groups are bulky,¹² they are possibly not large enough to shield all -OH groups and therefore SiO₂-TiCl₂ (914 cm⁻¹) and some SiO-TiCl₃ (1014 cm⁻¹) can still form on the surface. It could also be that islands of H-bonded -OH groups exist on the surface, in which larger parts of the surface remain non-passivated. The amount of non-passivated -OH on the SiO₂ surface might be exacerbated by the structure of the nanoporous substrate. The smallest pores have an average diameter of ~5 nm,²⁵ and diffusion of the bulky DMATMS molecule (~7.4 Å) could be hindered in the most narrow pores. TiCl₄, which is significantly smaller (~4.3 Å), might have access to a larger number of -OH groups as well as more narrow pores. However, in semiconductor applications planar surfaces, or 3D patterns of larger size are typically used, through which diffusion of the DMATMS molecule should not be a limiting factor, as has been demonstrated for Ru ASD in nanopatterns.^{10, 13} To fully quantify inhibition, growth over an extended number of cycles is discussed in the *Inhibited TiO₂ ALD growth* section. Nonetheless, overall TiCl₄ reacts with only 23% of the available -OH groups in the first half-cycle.

A second possible mechanism for inhibition loss is degradation of the surface passivation layer. Minor decreases in the intensities of the C-H and Si-CH₃ vibrations (at 2961 cm⁻¹ and 1258 cm⁻¹, respectively) indicate that the -OSi(CH₃)₃ termination is relatively stable during the TiCl₄ and H₂O half-cycles. Overall, less than 4% of the initial -OSi(CH₃)₃ groups are removed during the first TiO₂ cycle, as indicated by analysis of the peak integrals for C-H stretch and Si-CH₃ rocking vibrational modes. Both precursors are necessary to remove the -OSi(CH₃)₃ termination. The decrease in the peak intensity of the C-H stretch vibrational modes (2961 cm⁻¹) during TiCl₄ exposure might indicate complexation of TiCl₄ and -OSi(CH₃)₃ surface groups. The decrease in the peak intensity of the Si-CH₃ rocking vibrational modes (1258 cm⁻¹) during H₂O exposure suggests the removal of a small fraction of the -OSi(CH₃)₃ groups.

The leaving group could take forms including $\text{Cl-Si(CH}_3)_3$ or $\text{H-Si(CH}_3)_3$. Further quantum chemical studies could shed more light on this inhibition loss mechanism. However, due to its limited extent, $-\text{OSi(CH}_3)_3$ removal is most likely not the most important contributor to inhibition loss.

E. DMATMS reaction on H-terminated Si

H-terminated Si is an inherently inhibiting surface for $\text{TiCl}_4/\text{H}_2\text{O}$ ALD.^{40, 41} To further increase the selectivity of the ALD process, we investigate whether the addition of DMATMS before ALD on H-terminated Si can improve inhibition (Figure 3). The FTIR spectrum for the H-terminated Si starting surface is shown in Figure 3a. H-terminated Si is exposed to DMATMS for up to 60 cycles to investigate the reaction between the two. The differential FTIR spectrum shows presence of absorbance peaks for C-H and Si-CH₃ (2961 cm^{-1} , 1258 cm^{-1}), which indicate the presence of an $-\text{OSi(CH}_3)_3$ termination on the surface after 5 cycles of DMATMS (Figure 3b). The $-\text{OSi(CH}_3)_3$ termination forms as a result of the reaction between DMATMS and residual isolated -OH groups on the H-terminated Si surface, as evidenced by the consumption of residual -OH groups (3735 cm^{-1}) and the formation of new Si-O-Si bonds ($1050\text{-}1060\text{ cm}^{-1}$, 850 cm^{-1}). The few residual -OH groups are all isolated and react quickly with DMATMS to form $-\text{OSi(CH}_3)_3$ termination. Therefore, $-\text{OSi(CH}_3)_3$ termination on H-terminated Si surfaces has the same formation mechanism as seen on hydroxylated SiO_2 .

We see a drastic increase in the peaks associated with $-\text{OSi(CH}_3)_3$ (2961 cm^{-1} , 1258 cm^{-1}) during the first 5 DMATMS cycles. The surface coverage of the $-\text{OSi(CH}_3)_3$ continues to increase until 30 cycles, after which it saturates (Figure 3c). Interestingly, this is paired with a decrease in the Si-H surface concentration (2100 cm^{-1} , 916 cm^{-1} , 665 cm^{-1}), which becomes prominent after 60 cycles. The reaction of DMATMS with non-activated Si-H bonds, i.e., without catalyst, is unlikely or would require the formation of more reactive Si atoms, for instance through decomposition into silylenes.^{42, 43} It is more likely that the continued reaction of DMATMS with the Si-H surface is related to the presence of a small amount of O on the surface, in other forms than residual -OH surface groups. O has been shown to remain in sub-monolayer quantities on HF-cleaned Si surfaces, even after full removal of the native oxide.^{44, 45} Surface O can be integrated into the Si surface as Si-O-Si bridges, into the backbone as O-Si-H, or more importantly, can insert itself into Si-H bonds to form Si-OH groups.^{28, 45} It is difficult to resolve the formation of new Si-O-Si bonds due to surface O, as these bonds are also formed by the reaction of DMATMS with -OH.

To confirm our hypothesis, we collected FTIR spectra of the porous H-terminated Si surface as soon as it was loaded into the reactor, and after it was annealed for 60 minutes at $250\text{ }^\circ\text{C}$. The differential spectrum shows the partial removal of Si-H surface termination, even without exposure to any precursor (Figure 4). The reduction is apparent for all Si-H_x ($x = 1, 2, 3$) types. The time evolution of the H-terminated Si starting surface also shows the generation of Si-O-Si bonds (1088 cm^{-1} , 850 cm^{-1}) and isolated -OH groups (3735 cm^{-1}) with residual O from the HF clean. There is no direct indication of O incorporation into the O-Si-H backbone as there are no clear peaks at associated wavenumbers (2273 cm^{-1} and 881 cm^{-1}).²⁸ The generation of Si-O-Si and Si-OH creates new reactive sites on the otherwise inherently passivated H-terminated Si surface. The presence of such a mechanism necessitates additional passivation approaches to improve ALD inhibition during ASD with H-terminated Si as non-growth area. Possibly, DMATMS might offer one such route of improving passivation.

This is the author's peer reviewed, accepted manuscript. However, the online version of record will be different from this version once it has been copyedited and typeset.
PLEASE CITE THIS ARTICLE AS DOI: 10.1116/1.50002493

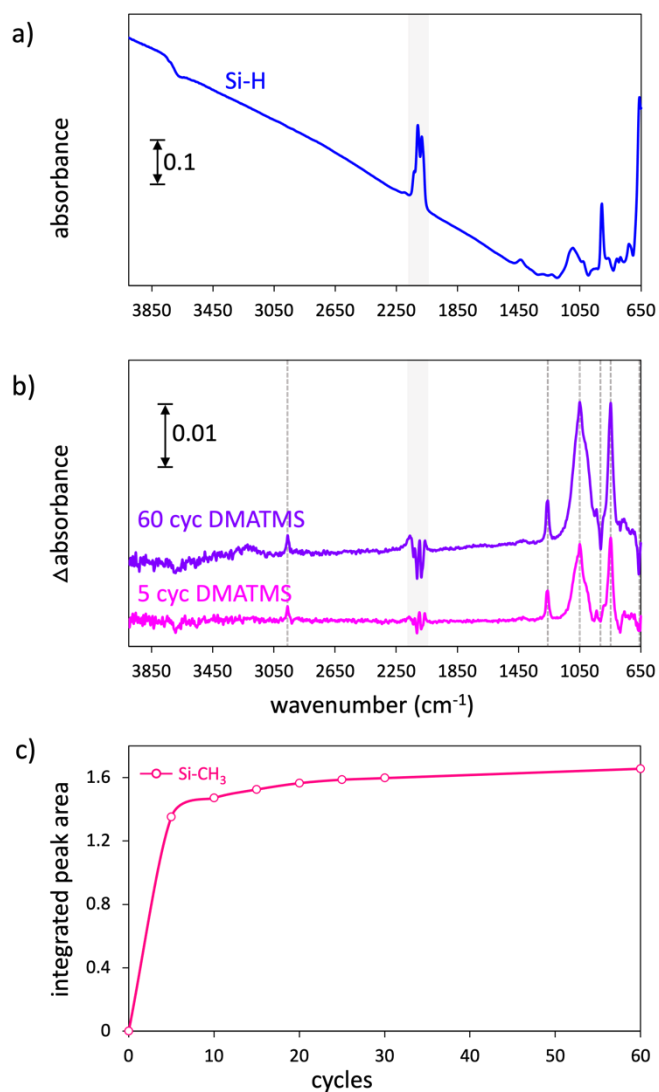


Figure 3 a) FTIR spectrum of starting SiO₂ surface, b) Differential FTIR spectra of the SiO₂ surface after 5 or 60 cycles DMATMS, integrated area under c) Integrated area of the SiCH₃ peak between 1282-1248 cm⁻¹ as function of TiCl₄/H₂O ALD cycles.

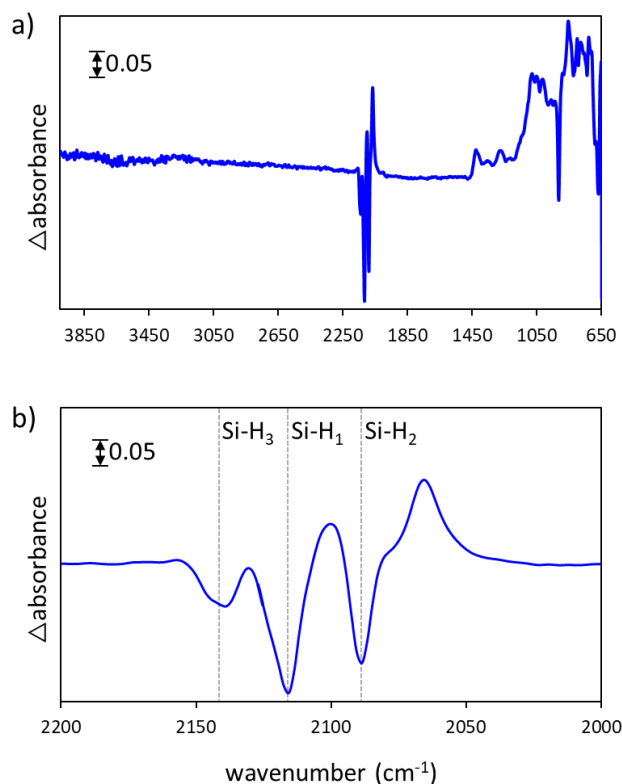


Figure 4 a) Differential FTIR spectrum of the H-terminated Si surface after a 60 minute anneal at 250 °C w.r.t. the surface as loaded into the reactor. b) close up of the spectrum between wavenumbers 2200 cm⁻¹ and 2000 cm⁻¹, with detailed assignment of the Si-H_x stretches for x = 1, 2, 3.²⁸

F. Surface reactions during the first TiCl₄/H₂O ALD cycle on H-terminated Si

Next, we study the surface reactions of TiCl₄/H₂O ALD on a non-passivated porous H-terminated Si surface (i.e., without DMATMS treatment). This is done to better understand the mechanisms by which DMATMS could provide additional passivation (Figure 5). Two mechanisms are responsible for inhibition loss. The first mechanism is the reaction of TiCl₄ with the small number of -OH groups on the surface (3760-3400 cm⁻¹). The surface -OH a combination of both residual -OH groups and the constant generation of -OH groups and Si-O-Si bridges on the surface, due to post-HF clean O on the surface. The second mechanism is the decrease in absorbance associated with Si-H during the first TiCl₄ half-cycle (2100 cm⁻¹, 916 cm⁻¹, 665 cm⁻¹). TiCl₄ is able to react directly with the Si-H surface. TiCl₄ can either displace the Si-H bond entirely to form Si-TiCl₃ and HCl, or kinetically more feasible, directly chlorinate the surface, which results in Si-Cl and HTiCl₃.⁴⁶ We cannot directly observe Cl-containing surface species in our FTIR spectra, as the corresponding absorptions occur below 700 cm⁻¹.^{29, 47} Subsequent exposure of Si-Cl to H₂O at 250 °C can either generate Si-O-Si bridges, or Si-OH groups.⁴⁷⁻⁴⁹ Some evidence for the formation of Si-O-Si can be found in the formation of the associated shoulders at 1088 cm⁻¹ and 850 cm⁻¹. Previous studies of the interaction of Si-Cl surfaces with H₂O have not observed the formation of -OH groups.^{47, 49} Nonetheless, we observe here that H₂O exposure also generates a small increase in the intensity of the -OH absorption (3700 cm⁻¹). Both siloxane bridges and -OH groups are potential reactive sites for TiCl₄, either by stimulating physisorption, or by direct reaction. Nonetheless, both the Si-O-Si and -OH vibrational signatures are very weak, and therefore only initiate slow growth during the first cycles of TiCl₄/H₂O ALD on H-terminated Si. Nonetheless, addition of a DMATMS pretreatment could further delay ALD growth.

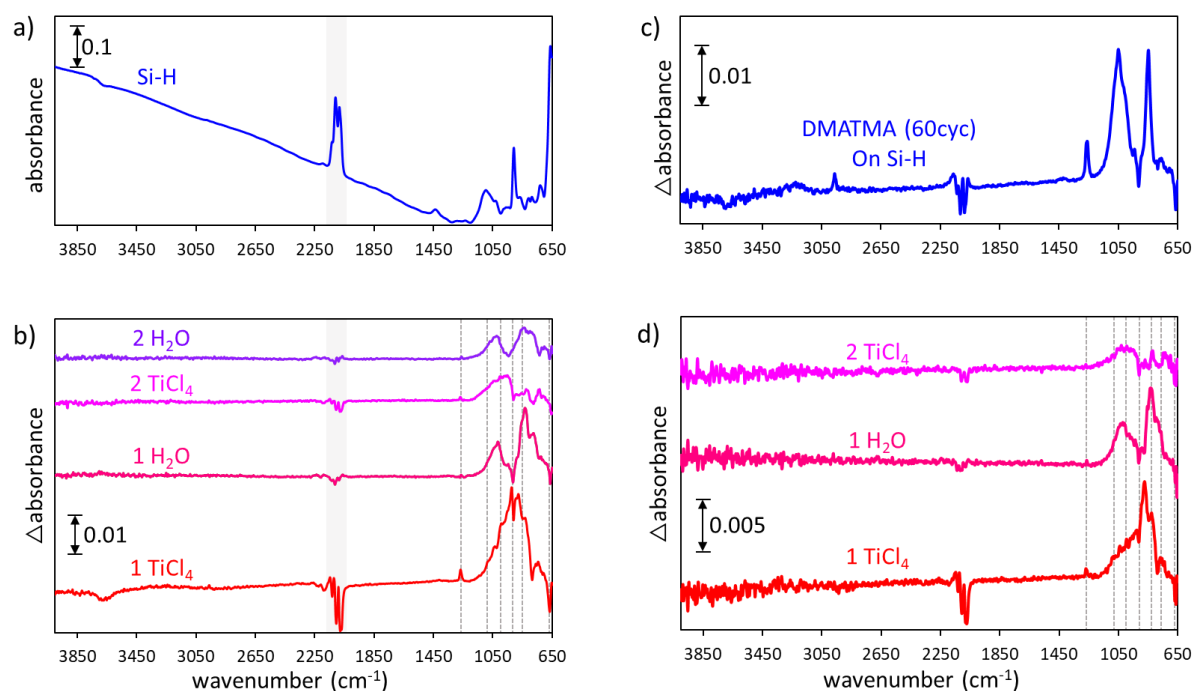


Figure 5 a) FTIR spectrum of the pristine H-terminated Si, b) differential spectra after TiCl_4 and H_2O half-cycles during the first 2 TiO_2 ALD cycles on H-terminated Si. c) FTIR spectrum after 60 cycles of DMATMS on the H-terminated Si. d) differential spectra after TiCl_4 and H_2O half-cycles during the first 2 TiO_2 ALD cycles on DMATMS-treated H-terminated Si.

G. Surface reactions during the first $\text{TiCl}_4/\text{H}_2\text{O}$ ALD cycle on passivated H-terminated Si

To investigate whether DMATMS exposure can further delay TiO_2 nucleation and growth, $\text{TiCl}_4/\text{H}_2\text{O}$ ALD is performed on the H-terminated Si after 60 cycles of DMATMS (Figure 5 **Error! Reference source not found.**). Remarkably, already in the first cycle, the adsorption of TiCl_4 is strongly repressed compared to the case without DMATMS, as evidenced by the lower peak intensity (Figure 5b, 1014 cm^{-1}). Also, in the subsequent H_2O and TiCl_4 exposures, the increase of the Ti-O-Ti absorbance intensity (810 cm^{-1} , 760 cm^{-1}) is only half that seen on the non-passivated H-terminated Si surface.

No decrease in absorbance is observed for the O-H stretch ($3760\text{--}3400\text{ cm}^{-1}$), which indicates that the number of -OH groups available for reaction with TiCl_4 is below the detection limit. This means that the -OH groups were fully passivated by the DMATMS exposure. There is also no decrease in absorption associated with the $-\text{OSi}(\text{CH}_3)_3$ termination during TiCl_4 and H_2O exposures (2961 cm^{-1} , 1258 cm^{-1}) during the first two TiO_2 ALD cycles. This indicates that the $-\text{OSi}(\text{CH}_3)_3$ termination is not removed in any significant amount from the H-terminated surface. This is in contrast to passivated SiO_2 , on which loss of $-\text{OSi}(\text{CH}_3)_3$ termination was observed during the first two TiO_2 ALD cycles. There is, however, again decreased absorbance for the peaks associated with Si-H, which indicates the loss of Si-H termination (2100 cm^{-1} , 916 cm^{-1} , 665 cm^{-1}). There is no mechanism by which DMATMS would protect the Si-H surface bonds from reaction with TiCl_4 . It seems that the inhibition loss is completely due to Si-H reactivity and can be linked back to the same mechanisms discussed above for non-passivated H-terminated Si.

Overall, by fully eliminating the -OH-related passivation loss mechanism, TiO_2 growth is significantly reduced with respect to the non-passivated case. As we discussed above, the enhanced Ti content in the first ALD cycle on passivated SiO_2 is an important factor in the

number of TiO_2 nuclei formed on the non-growth surface. Identically, on H-terminated Si limiting the number of those nuclei in the first cycle is an important mechanism by which DMATMS exposure decreases overall defectivity.

Finally, we cannot fully exclude the presence of residual Si-F bonds after the HF-treatment of the samples. We do not expect any reaction between any potential Si-F bonds and DMATMS. However, these bonds are easily hydrolyzed upon exposure to H_2O , which results in the formation of -OH bonds on the surface.⁵⁰ If a significant amount of Si-F bonds are present on the H-terminated Si surface, a DMATMS treatment after the first H_2O half-cycle could improve selectivity. Yet, Si-F bond occur at too low wavenumbers to be measured in our setup.

H. Inhibited TiO_2 ALD growth

To properly assess growth inhibition on the four studied surfaces, we quantified the TiO_2 ALD growth over 150 cycles by RBS (Figure 6). On the non-passivated SiO_2 , growth in the first 10 cycles is characterized by a large average GPC value of 0.036 nm cy^{-1} , which settles into steady state growth with a GPC of 0.027 nm cy^{-1} . This is in line with the enhanced growth rate also seen with FTIR during the first ALD cycle.

Of the three inhibiting surfaces, nucleation and growth proceeds fastest on the H-terminated Si substrate. This is in line with the two inhibition loss mechanisms identified for this surface, namely due to the reactions of TiCl_4 with residual isolated -OH groups and with Si-H bonds. Slightly longer inhibition is offered by the DMATMS-passivated SiO_2 substrate. Inhibition loss during the very first ALD cycles is likely mostly due to the presence of residual H-bonded -OH groups on the surface, resulting mostly in TiCl_2 surface species. After the first ALD cycles, additional nucleation is still possible through minor reaction of the ALD precursors with the $-\text{OSi}(\text{CH}_3)_3$ termination.

The longest growth delay is offered by the DMATMS-passivated H-terminated substrate. The passivation of all initial -OH sites on the surface is sufficient to keep the TiO_2 thickness below the RBS detection limit ($\pm 0.1 \text{ nm}$) after 10 cycles. Eventually, inhibition is lost through one of two mechanisms. First, through the reaction of TiCl_4 with the Si-H bonds, resulting in Si-Cl surface species, which can be hydrolyzed by H_2O . Second, through the generation of new nucleation sites by the incorporation of post-HF clean O into -OH groups and Si-O-Si bridges. Overall, a substantial growth delay is achieved by applying the DMATMS treatment on both the SiO_2 and H-terminated Si surfaces: after 75 ALD cycles only $0.26 \pm 0.08 \text{ nm}$ and $0.22 \pm 0.07 \text{ nm}$ of TiO_2 is deposited on the DMATMS passivated SiO_2 and H-terminated Si substrates, respectively. These numbers are significant improvements over the $1.60 \pm 0.11 \text{ nm}$ and $0.69 \pm 0.09 \text{ nm}$ of TiO_2 for the untreated SiO_2 and H-terminated Si substrates after 75 cycles. After 100 ALD cycles, the steady-state GPC of 0.03 nm cy^{-1} is reached on all surfaces.

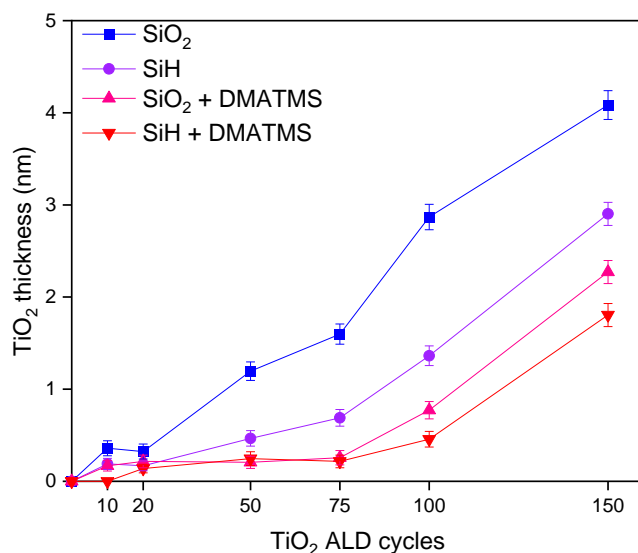


Figure 6 Equivalent TiO₂ film thickness as a function of ALD cycles, as measured by RBS on planar samples.

I. Considerations for ASD process design

Based on our findings, some recommendations and limitations concerning TiO₂ ASD with SiO₂ or H-terminated Si as the non-growth area can be discussed. Firstly, on SiO₂, the addition of DMATMS in an ABC-type cycle with A = DMATMS, B = TiCl₄, and C = H₂O will most likely not result in a significant advantage over a simple DMATMS pretreatment. The reaction of -TiCl₃ and -TiCl₂ with H₂O in the second half-cycle results in the formation of vicinal, H-bonded -OH groups, which do not react significantly with DMATMS. Previous work has already shown that DMATMS is unable to passivate TiO₂ surfaces.¹⁵ Therefore, passivation of TiO₂ nuclei by DMATMS is unlikely and selectivity improvements should revolve around preventing nucleation. Instead, a supercycle TiO₂ ASD process can be proposed in which SiO₂ is the non-growth area. Such a supercycle should consist of 60 cycles of DMATMS, 75 cycles of TiCl₄/H₂O ALD, an atomic layer etching (ALE) step and a hydroxylation step. We believe that applying a short ALE step after 75 ALD cycles should be sufficient to fully remove deposition of the DMATMS-passivated SiO₂ non-growth area. Several selective TiO₂ ALE processes have already been developed.^{41, 51-54} The hydroxylation step (e.g., an O plasma) is necessary to ensure that the surface can be repassivated by DMATMS.⁵⁵

If H-terminated Si is the non-growth area, an ABC-type cycle could increase selectivity. As discussed above, there is constant generation of -OH groups and Si-O-Si bridges on the surface, due post-HF clean O. This constantly creates new potential ALD nucleation sites. The addition of a DMATMS pulse at the start of each cycle could mitigate this nucleation site generation mechanism by passivating all newly generated -OH groups. Alternatively, a high temperature bake (> 1000 °C) in H₂ atmosphere is also able to remove any surface O before ALD.⁵⁶ However, the usage thereof is restricted by the thermal budget of the process. Finally, to ensure high selectivity and prevent TiO₂ nucleation on the DMATMS-passivated H-terminated Si, a Ti-precursor should be selected that does not react with Si-H bonds. By applying the above recommendations, the selectivity of TiO₂ ASD processes with SiO₂ or H-terminated Si as the non-growth area should be improved.

IV. CONCLUSIONS

In this paper, we have studied the interactions of DMATMS with SiO₂ and H-terminated Si surfaces, as well as with TiCl₄ and H₂O precursors in the context of highly selective ASD. We have shown that DMATMS reacts with isolated -OH groups on H-terminated Si and SiO₂

surfaces. $\text{TiCl}_4/\text{H}_2\text{O}$ ALD was shown to nucleate on both isolated and H-bonded -OH groups on both surfaces. Interestingly, we showed that the extent of rehydroxylation during the first H_2O exposure is limited, which in turn limits subsequent TiCl_4 uptake. Based on this insight, highly selective ASD should be achievable by preventing TiCl_4 adsorption mainly during the first TiCl_4 exposure.

On DMATMS-passivated SiO_2 , the mechanism of inhibiting TiO_2 ALD on SiO_2 is firstly through limiting the number of initial reactive -OH groups and therefore also the number of TiO_2 nuclei. As mentioned above, the extent of rehydroxylation during ALD is reduced which limits particle growth after nucleation.

DMATMS is unable to passivate all -OH sites on the nanoporous SiO_2 , either through steric hindrance of the bulky $-\text{OSi}(\text{CH}_3)_3$ group, or through non-reactive H-bonded -OH groups. Still, less than a quarter of these non-passivated -OH groups are reactive during TiCl_4 exposure. The fact that so few -OH groups react during TiCl_4 exposure further supports the importance of steric shielding by the $-\text{OSi}(\text{CH}_3)_3$ groups. A finding that is also supported by a recent study by Xu et al. of Al_2O_3 ALD on DMATMS-treated SiO_2 . However, in their studies, Xu et al. found that a major contribution loss mechanism was physisorption of the Al-precursor on siloxane bridges, which we don't find for our system.¹⁸

On the inherently inhibiting H-terminated Si surface, we showed how two mechanisms lead to inhibition loss, namely residual and generated -OH groups, and TiCl_4 interaction with Si-H bonds. A great improvement in TiO_2 ALD inhibition is achieved when the H-terminated Si surface is combined with DMATMS passivation. DMATMS improves inhibition through the full passivation of the residual -OH groups on the H-terminated Si surface. As $-\text{OSi}(\text{CH}_3)_3$ groups have been shown to inhibit many ALD processes, the usage of DMATMS on H-terminated Si can be expected to improve selectivity for many ASD processes where this surface is the non-growth area.

This study illustrates the importance of determining the reactive sites of SMIs and ALD precursors in passivation schemes for rational ASD process design. A further study of the interaction of alternative Ti-precursors with the $-\text{OSi}(\text{CH}_3)_3$ termination and SiO_2 and H-terminated Si surfaces should enable further TiO_2 ASD selectivity improvements, in a way that is fully compatible with ASD supercycles.

ACKNOWLEDGEMENTS

The Authors acknowledge support from the Electronic Component Systems for European Leadership Joint Undertaking under the grant agreement No. 692522. The authors also acknowledge funding from the Semiconductor Research Corporation, Task 2974.001.

AUTHOR DECLARATIONS

Conflict of Interest

The Authors have no conflicts to disclose.

Data Availability

The data that support the findings of this study are available from the corresponding author upon reasonable request.

REFERENCES

1. A. J. M. Mackus, M. J. M. Merckx and W. M. M. Kessels, *Chemistry of Materials*, 2019, **31**, 2-12.
2. G. N. Parsons and R. D. Clark, *Chemistry of Materials*, 2020, **32**, 4920-4953.
3. J. Yarbrough, A. B. Shearer and S. F. Bent, *Journal of vacuum science & technology. A, Vacuum, surfaces, and films*, 2021, **39**, 21002.
4. F. S. M. Hashemi, C. Prasittichai and S. F. Bent, *Journal of Physical Chemistry C*, 2014, **118**, 10957-10962.
5. F. S. M. Hashemi, B. R. Birchansky and S. F. Bent, *Acs Applied Materials & Interfaces*, 2016, **8**, 33264-33272.
6. L. Lecordier, S. Herregods and S. Armini, *Journal of Vacuum Science & Technology A*, 2018, **36**.
7. M. Pasquali, S. Sergeant, T. Conard, V. Spampinato, A. Viva, S. De Gendt and S. Armini, *ACS Appl. Electron. Mater*, 2021, **3**, 2622-2630.
8. H. P. Chen, Y. H. Wu, H. Y. Huang, C. H. Tsai, S. K. Lee, C. C. Lee, T. H. Wei, H. C. Yao, Y. C. Wang, C. Y. Liao, H. K. Chang, C. W. Lu, W. S. Shue and M. Cao, San Francisco, 2021.
9. A. Mamei, M. J. M. Merckx, B. Karasulu, F. Roozeboom, W. M. M. Kessels and A. J. M. Mackus, *ACS Nano*, 2017, **11**, 9303-9311.
10. J. Soethoudt, H. Hody, V. Spampinato, A. Franquet, B. Briggs, B. T. Chan and A. Delabie, *Advanced Materials Interfaces*, 2019, **6**.
11. J. J. Fripiat, J. Uytterhoeven, U. Schobinger and H. Deuel, *Helvetica Chimica Acta*, 1960, **23**, 7.
12. R. Khan, B. Shong, B. G. Ko, J. K. Lee, H. Lee, J. Y. Park, I. K. Oh, S. S. Raya, H. M. Hong, K. B. Chung, E. J. Lubner, Y. S. Kim, C. H. Lee, W. H. Kim and H. B. R. Lee, *Chemistry of Materials*, 2018, **30**, 7603-7610.
13. J.-W. J. Clerix, E. A. Marques, J. Soethoudt, F. Grillo, G. Pourtois, J. R. Van Ommen and A. Delabie, *Advanced materials interfaces*, 2021.
14. J. Soethoudt, F. Grillo, E. A. Marques, J. R. van Ommen, Y. Tomczak, L. Nyns, S. Van Elshocht and A. Delabie, *Advanced materials interfaces*, 2018, **5**, 1800870-n/a.
15. J. Soethoudt, Y. Tomczak, B. Meynaerts, B. T. Chan and A. Delabie, *Journal of Physical Chemistry C*, 2020, **124**, 7163-7173.
16. Y. Au, Y. Lin, H. Kim, E. Beh, Y. Liu and R. G. Gordon, *Journal of the Electrochemical Society*, 2010, **157**, D341-D345.
17. F. Grillo, J. Soethoudt, E. A. Marques, L. de Martin, K. Van Dongen, J. R. Van Ommen and A. Delabie, *Chemistry of Materials*, 2020, **32**, 12.
18. W. Xu, M. G. N. Haeve, P. C. Lemaire, K. Sharma, D. M. Hausmann and S. Agarwal, *Langmuir*, 2022, **38**, 652-660.
19. W. Xu, R. J. Gasvoda, P. C. Lemaire, K. Sharma, D. M. Hausmann and S. Agarwal, *Journal of vacuum science & technology. A, Vacuum, surfaces, and films*, 2022, **40**.
20. R. A. Nye, K. Van Dongen, H. Oka, H. Furutani, G. N. Parsons, D. De Simone and A. Delabie, San Jose, CA, USA, 2022.
21. M. J. M. Merckx, A. Angelidis, A. Mamei, J. Li, P. C. Lemaire, K. Sharma, D. M. Hausmann, W. M. M. Kessels, T. E. Sandoval and A. J. M. Mackus, *J. Phys. Chem. C*, 2022, **126**, 4845-4853.
22. J. Yarbrough, F. Pieck, D. Grigjanis, I.-K. Oh, P. Maue, R. Tonner-Zech and S. F. Bent, *Chem. Mater*, 2022, **34**, 4646-4659.

23. M. J. M. Merckx, R. G. J. Jongen, A. Mameli, P. C. Lemaire, K. Sharma, D. M. Hausmann, W. M. M. Kessels and A. J. M. Mackus, *Journal of Vacuum Science & Technology A*, 2021, **39**.
24. R. A. Nye, S. K. Song, K. Van Dongen, A. Delabie and G. N. Parsons, *Applied physics letters*, 2022, **121**.
25. H. Saare, G. Dianat and G. N. Parsons, *J. Phys. Chem. C*, 2022, **126**, 7036-7046.
26. B. Gong, Q. Peng and G. N. Parsons, *J. Phys. Chem. B*, 2011, **115**, 5930-5938.
27. B. Gong and G. N. Parsons, *Journal of Materials Chemistry*, 2012, **22**, 15672-15682.
28. D. B. Mawhinney, J. A. Glass and J. T. Yates, *J. Phys. Chem. B*, 1997, **101**, 1202-1206.
29. J. B. Kinney and R. H. Staley, *Journal of Physical Chemistry*, 1983, **87**, 3735-3740.
30. L. T. Zhuravlev and V. V. Potapov, *RUSSIAN JOURNAL OF PHYSICAL CHEMISTRY*, 2006, **80**, 1119-1128.
31. P. J. Launer and B. Arkles, in *Silicon Compounds: Silanes & Silicones*, Gelest, Inc., Morrisville, 2013, pp. 175-178.
32. S. E. Atanasov, PhD in Chemical Engineering, North Carolina State University, 2015.
33. A. R. Chowdhuri, C. G. Takoudis, R. F. Klie and N. D. Browning, *Applied Physics Letters*, 2002, **80**, 4241-4243.
34. B. B. Burton, S. W. Kang, S. W. Rhee and S. M. George, *J. Phys. Chem. C*, 2009, **113**, 8249-8257.
35. A. B. D. Nandiyanto, R. Oktiani and R. Ragadhita, *Indonesian Journal of Science & Technology*, 2019, **4**, 22.
36. S. Haukka, E. L. Lakomaa and A. Root, *Journal of Physical Chemistry*, 1993, **97**, 5085-5094.
37. K. B. Ramos, G. Clavel, C. Marichy, W. Cabrera, N. Pinna and Y. J. Chabal, *Chemistry of Materials*, 2013, **25**, 1706-1712.
38. R. L. Puurunen, *Chemical Vapor Deposition*, 2005, **11**, 79-90.
39. G. N. Parsons, *Journal of Vacuum Science & Technology A*, 2019, **37**.
40. H. Saare, S. K. Song, J.-S. Kim and G. N. Parsons, *Journal of applied physics*, 2020, **128**, 105302.
41. S. K. Song, H. Saare and G. N. Parsons, *Chemistry of Materials*, 2019, **31**, 4793-4804.
42. R. Becerra, J. P. Cannady and R. Walsh, *Phys Chem Chem Phys*, 2013, **15**, 5530-5538.
43. R. Rodriguez, Y. Contie, R. Nougue, A. Baceiredo, N. Saffon-Merceron, J.-M. Sotiropoulos and T. Kato, *Angew. Chem*, 2016, **128**, 14567-14570.
44. A. Ermolieff, F. Martin, A. Amouroux, S. Marthon and J. F. M. Westendorp, *Semiconductor science and technology*, 1991, **6**, 98-102.
45. S. Jayachandran, A. Delabie, A. Billen, H. Dekkers, B. Douhard, T. Conard, J. Meersschaut, M. Caymax, W. Vandervorst and M. Heyns, *Applied surface science*, 2015, **324**, 251-257.
46. M. K. Ghosh and C. H. Choi, *Chemical Physics Letters*, 2008, **461**, 249-253.
47. M. L. Wise, O. Sneh, L. A. Okada and S. M. George, *Surface science*, 1996, **364**, 367-379.
48. G.-Y. Fang, L.-N. Xu, L.-G. Wang, Y.-Q. Cao, D. Wu and A.-D. Li, *Nanoscale Res Lett*, 2015, **10**, 1-7.
49. S. Rivillon, R. T. Brewer and Y. J. Chabal, *Applied Physics Letters*, 2005, **87**, 3.
50. G. S. Higashi, Y. J. Chabal, G. W. Trucks and K. Raghavachari, *Applied Physics Letters*, 1990, **56**, 656-658.
51. P. C. Lemaire and G. N. Parsons, *Chemistry of Materials*, 2017, **29**, 6653-6665.
52. S. K. Song, J.-S. Kim, H. R. M. Margavio and G. N. Parsons, *ACS Nano*, 2021, **15**, 12276-12285.
53. S. M. George and Y. Lee, *Acs Nano*, 2016, **10**, 4889-4894.



This is the author's peer reviewed, accepted manuscript. However, the online version of record will be different from this version once it has been copyedited and typeset.
PLEASE CITE THIS ARTICLE AS DOI: 10.1116/1.50002493

54. Y. Lee, C. Huffman and S. M. George, *Chemistry of Materials*, 2016, **28**, 7657-7665.
55. J. Soethoudt, S. Crahaij, T. Conard and A. Delabie, *J. Mater. Chem. C*, 2019, **7**, 11911-11918.
56. H. Bender, S. Verhaverbeke, M. Caymax, O. Vatel and M. M. Heyns, *Journal of applied physics*, 1994, **75**, 1207-1209.

